SAND2019-15260C
Proceedings of the ASME 2020
14th International Conference on Energy & Sustainability
ES2020
June 8-10, 2020, Denver, CO, USA

ES2020-1620

OPERATIONAL MODES AND SYSTEM DESIGN OF A 2.0 MW_{TH} SODIUM MOLTEN SALT PILOT SYSTEM

Kenneth M. Armijo[1], Matthew D. Carlson[1], Dwight S. Dorsey[2], Joshua M. Christian[1] and Craig S. Turchi[3]

[1]Concentrating Solar Power Department, Sandia National Laboratories, Albuquerque NM, USA.
[2]Bridgers and Paxton, Albuquerque, NM, USA.
[3]National Renewable Energy Laboratory, Golden, CO, USA.

ABSTRACT

Nitrate molten salt concentrating solar power (CSP) systems are currently deployed globally and are considered state-of the art heat transfer fluids (HTFs) for present day high-temperature operation. Although slightly higher limits may be possible with molten salt, to fully realize SunShot efficiency goals of \$15/kWh$_{th}$ HTFs and an LCOE of 6¢/kWh, HTF technologies working at higher temperatures (e.g., 650 °C to 750 °C) will require an alternative to molten salts, such as with alkali metal systems. This investigation explores the development of a 2.0 MW$_{th}$ sodium receiver system that employs a sodium receiver as the HTF, as well as with a ternary chloride (20%NaCl/40%MgCl/40%KCl by mol wt.%) salt as a thermal energy storage (TES) medium to facilitate a 6-hr. storage duration. A sodium-to-salt heat exchanger model as well as a salt-to-sCO$_2$ primary heat exchanger model are employed and evaluated in this investigation. A thermodynamic system design model was developed using Engineering Equation Solver (EES) where state properties were calculated at inlets and outlets along both hot and cold legs of the pilot-scale plant. This investigation assesses receiver performance as well as system efficiency studies for the pump and system operational ranges. Results found that high efficiency sodium receivers were found to have higher heat transfer coefficients and required far less spreading of incident flux. The system performance model results suggest that for a pump speed of 2400 RPM, respective hot and cold pump TDH values were determined to be 260.1-307 ft. and 260.1-307 ft for pump flow rates of 90-120 GPM.

1. INTRODUCTION

The properties of sodium suggest that 90%+ efficient concentrating solar power (CSP) receivers can be designed at temperatures compatible with Gen3 CSP plants to improve overall thermodynamic system efficiencies [1]. A configuration that uses chloride salt storage with sodium as the heat transfer fluid (HTF) in the receiver is planned at Sandia's NSTTF. Sodium receivers tolerate higher flux than do chloride salt receivers, primarily due to creep-fatigue considerations at elevated temperatures. The high conductivity alleviates the thermal stress issues by reducing front-to-back receiver tube temperature differences [2]. It also improves heat transfer and allows a receiver to maintain an acceptable temperature difference between the absorber inner surface and the fluid [3]. Sodium is more forgiving than salt with regards to the risk of freezing, which is an advantage over salt in the receiver. However, it is a hazardous material, and within the CSP community is yet to gain widespread acceptance. Nonetheless, pilot scale plants using sodium have operated successfully, such as the 1.2 MW$_e$ Vast Solar facility [3]. The 1.1 MW Vast Solar Jemalong plant in Australia uses liquid sodium as an HTF, with 3 hours of storage, to heat steam and power turbine generators [6]. VAST Solar's Jemalong plant uses 5 individual, small, 30m towers with the intention of demonstrating modular applications of their systems. More thermally efficient receivers employing HTFs such as sodium may be required to fully realize the SunShot LCOE target of 6¢/kWh [4]. While liquid alkali metals are promising for receivers, they are less suitable as storage media due to their lower heat capacity and higher material cost compared to high-temperature molten salt alternatives [5]. The Gen 3 Liquid-Pathway team, comprised of various research institutions and led by NREL, are developing a CSP system to advance liquid-phase systems technology from the current state of-the-art solar-salt/Steam Rankine design embodied by industrial plants [3] operating at 565 °C and ~42% thermo-electric conversion efficiency. This work describes a next-generation CSP system design with a salt or alkali metal HTF capable of interfacing with a supercritical carbon dioxide (sCO$_2$) Brayton cycle operating at 720 °C and ~50% efficiency. A system model design, for a 2.0-MW$_{th}$ test loop has been developed with a target receiver temperature of 735 °C, as well

Sandia National Laboratories is a multimission laboratory managed and operated by National Technology & Engineering Solutions of Sandia, LLC, a wholly owned subsidiary of Honeywell International Inc., for the U.S. Department of Energy's National Nuclear Security Administration under contract DE-NA0003525.

as hot and cold tank storage temperatures of 720 °C and 500 °C respectively.

The system design includes liquid sodium employed as an HTF for a receiver loop section, which for this model also includes an EM pump and sodium-to-salt heat exchanger (HX). A more detailed description of the salt-side of the system model can be found in Armijo et al. [6] where the sodium-to-salt HX is connected to a riser and downcomer thermal transport system that circulates salt to a 120 ft. platform atop a solar tower. The ternary chloride molten salt is used as the TES media for 6 hours. To facilitate the required storage duration and thermal heat input, the calculated mass flow rate of the sodium is 5.73 kg/s, which requires a 33,072-gallon salt TES inventory. To facilitate thermal transport between the receiver and the TES, a piping and flow control system has been designed to ensure a $1MW_{th}$ heat input to a salt/sCO_2 heat exchanger that provides thermal input to an sCO_2 Brayton power cycle. Operational modes investigated include steady state operation, as well as transient start-up, shut-down and idle modes. In this work, engineering design has been performed for a Pilot-scale test system operated at Sandia National Laboratories. Comparison is made between this system and one using a chloride molten salt, with a 20%NaCl/40%MgCl/40%KCl mole percent composition. This research also investigates performance for a scaled $100MW_{Net}$ system, employing sodium as the receiver HTF, operating under the same investigated operational modes.

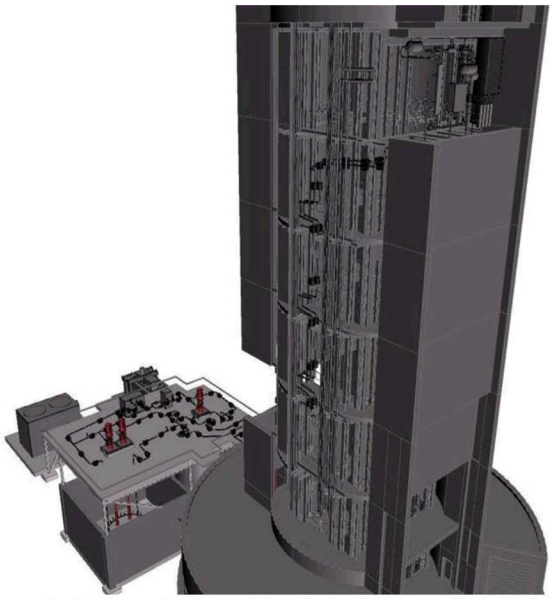

Figure 1. 3-D rendering of the Solar Tower pilot-scale system.

With sodium's thermal conductivity being approximately two orders of magnitude higher, substantially increased CSP receiver efficiencies may also be possible. For this investigation comparison studies will be performed across all operational modes to assess impacts related to total dynamic head (TDH) and pressure drops across major components, such as the receiver, heat exchanger, downcommer and riser. The TDH values are used for sizing of respective system and pump operational curves. The total length of piping used in the system is tentatively calculated to be 833 ft with a 2.5 in. Sch. 80 NPS, composed of Sch. 80, Inconel 617 alloy for the hot leg, and SS347H for the cold leg. Heat losses along the respective flow-legs are evaluated with respect to total system efficiency.

2. SYSTEM PROCESS DESIGN MODELLING

A thermodynamic system design model was developed using Engineering Equation Solver (EES) where state properties were calculated at inlets and outlets, and along both hot and cold legs of a pilot-scale plant. For this investigation, a steady-state model was developed for the thermal-hydraulic system. User-supplied inputs and calculation settings are supplied through the EES diagram window and via lookup tables, as well as parametric tables as appropriate for the solution configuration. Data from any user input method can be saved to and loaded from a file to simplify scenario modeling without requiring multiple copies of the EES code itself. Although several transient operational modes are presently being developed with respect to start-up and shut-down operational modes, this investigation only considers the stead operation of the final attemporation mode.

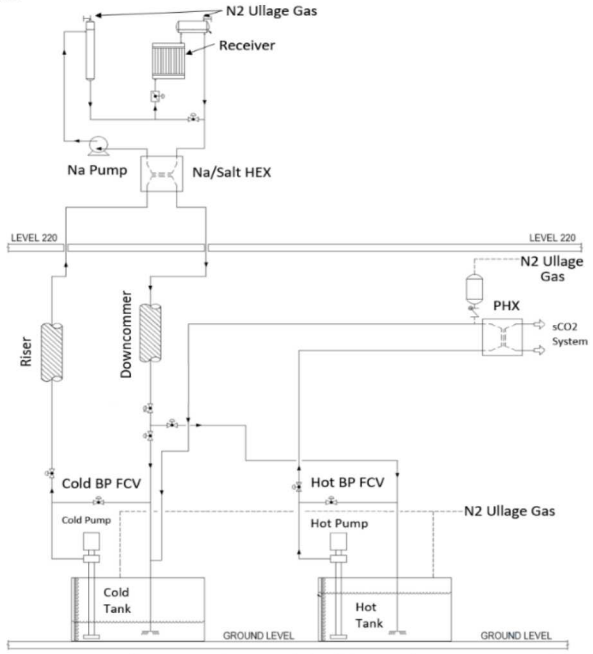

Figure 2. Sodium-Molten chloride salt P&ID with EES thermodynamic state points.

This system was modelled with flow from the cold tank at the base of tower (inset picture), up a riser test section to a sodium to molten salt heat exchanger (HX) section at the 120 ft. level of the NSTTF solar tower. The salt is then expected to flow down a downcomer hot leg to a hot salt tank, operated at 720 □. The salt then flows to a primary heat exchanger which transfer up to 1 MWth of heat to an sCO_2 loop (not discussed here). The salt then flows back at a lower 500 □ temperature to the cold tank. For the receiver section, an electro-magnetic pump circulates liquid sodium through a receiver inlet vessel to a sodium receiver

where it is heated as high as 750 □. The sodium then passes through an outlet receiver vessel and back to the sodium/salt HX. Various approximations were made with this simplified process flow design, such as omission of an attemporation pump, heater control characteristics and tank thermal management. Additionally, sodium system components such as cold fingers, vapor traps, scrubbers, etc. are also not included in this study. For the TES, the ternary chloride salt was considered due to its lower melting point, higher heat capacity, and lower cost than binary chloride salt chemistries, where other salts have been shown to be too expensive, unstable, or have substantial vapor pressure [4].

Additionally, for this investigation a simplified tubular receiver model was determined necessary as part of the system modeling effort to develop a "digital twin" of the Generation 3 molten salt Concentrating Solar Power (Gen3CSP) liquid pathway pilot plant [6]. This model must solve for the expected outlet conditions of the receiver heat transfer fluid (HTF) in addition to the peak receiver surface temperature based on an incident solar flux from the heliostat field, the inlet conditions of the HTF, and primary design parameters of the receiver such as the number and size of tubes used. Considerations for fluid, structural, heat transfer, and optical design in addition to required design elements such as the lower and upper manifolds will not be captured in this model and must be addressed in more detailed models.

3. DISCUSSION & RESULTS

3.1. Receiver Characterization

A receiver parametric study was performed investigating the required flux needed to achieve a 2.0 MWth operation under uniform flux spreading. This work considered both the ternary chloride molten salt and sodium as the HTF. This analysis is ideal since in reality, even with a multiple point aiming strategy variations in the flux profile are likely. In lieu of model validation data limitations on receiver performance, as modeled based on work by Ho.[7], the thermal efficiency of any receiver can be described by Eqn. 1 as the ratio of the net heat into the receiver fluid to the incident heat provided to the receiver, including reflectance, external convection, and radiative losses. Optical considerations for field efficiency and spillage are not considered and the incident flux is assumed uniform across the receiver surface. The heat absorbed by the HTF can be estimated by Eqn. 2 assuming that the heat transfer coefficient (HTC) and the heat flux are relatively uniform resulting in the receiver and fluid temperatures being assumed to be the average temperatures along the receiver.

$$\eta_{th} = \frac{\dot{q}''_{in} - \dot{q}''_{loss}}{\dot{q}''_{in}} = \frac{\dot{q}''_{in} - \dot{q}''_{ref} - \dot{q}''_{conv} - \dot{q}''_{rad}}{\dot{q}''_{in}} = \frac{\dot{q}''_{abs}}{\dot{q}''_{in}} \quad (1)$$

$$\dot{q}''_{abs} = htc(T_R - T_F) \quad (2)$$

These equations allow the limits to receiver performance to be modeled as shown in Figure 3 given reasonable values for receiver absorptance, emissivity, external convective heat transfer coefficient, ambient temperature, and average fluid temperature. A maximum receiver efficiency can be seen for each value of HTF heat transfer coefficient which require different levels of concentration to achieve. Based on the peak efficiencies it is also likely that an incident flux above 5000 kW/m^2 will result in excessive receiver surface temperatures without dramatically higher heat transfer coefficients.

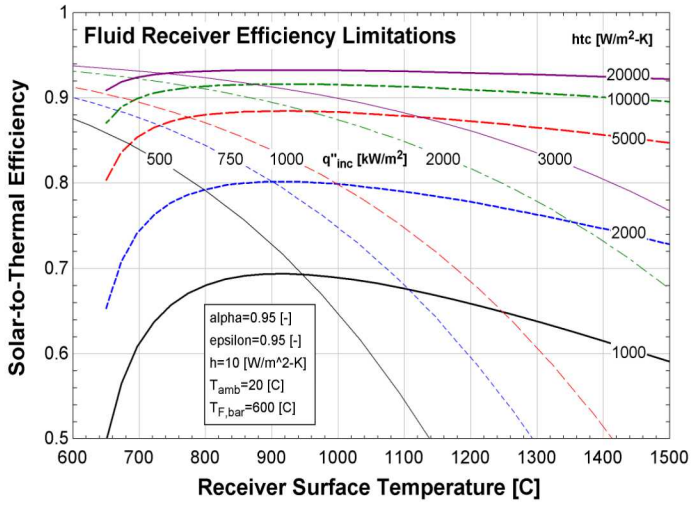

Figure 3. Limits to solar receiver efficiency using convective fluid cooling with contours shown for incident flux and fluid heat transfer coefficient versus the receiver surface temperature under the assumptions shown.

The HTC and pressure drop per unit length of a liquid vary primarily with mass flux and to a lesser extent with temperature, pressure, and flow geometry. Assuming a liquid receiver operating near ambient pressure with a tube size of ½ NPS Sch.10, the trends in heat transfer coefficient and pressure drop can be calculated as shown in **Figure** . 4 and **Figure** 5.

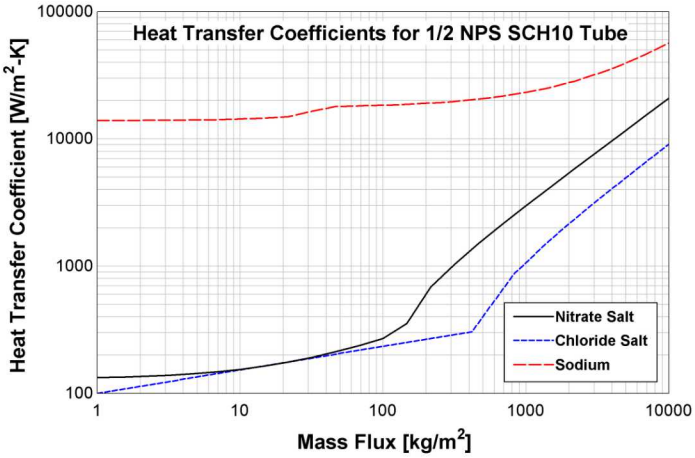

Figure 4. Heat transfer coefficient for several fluids versus mass flux at 600 C and ambient pressure. The nitrate salt used is a mixture of 60% $NaNO_3$ and 40% KNO_3 and the chloride salt used is a mixture of 20% NaCl, 40% KCl, and 40% $MgCl_2$.

Depending on the height and configuration of the receiver, the pressure drop per unit length allowed will range from 0.1 bar/m to 0.5 bar/m resulting in expected mass fluxes between 3000 kg/m^2 and 10000 kg/m^2 because the pressure drop of the three fluids considered is fairly similar. The resulting heat transfer coefficients however are very different, with nitrate salts ranging from 8,000 to 20,000 W/m^2-K, chloride salts ranging from 3,000 to 9,000 W/m^2-K, and sodium ranging from 30,000 to 60,000 W/m^2-K. Comparing these values with Figure these ranges suggest that while nitrate salt receivers can potentially reach between 85% and 95% efficiencies, the ternary chloride salt used will be limited to between 80% and 90% efficiency. Liquid sodium, however, can easily maintain efficiencies above 90% and up to 95% provided sufficient flux can be provided to the receiver but the concentration ratio may artificially limit the capability of a sodium receiver. These high heat transfer coefficients also allow the receiver surface temperature to reach a minimum while still achieving high efficiencies.

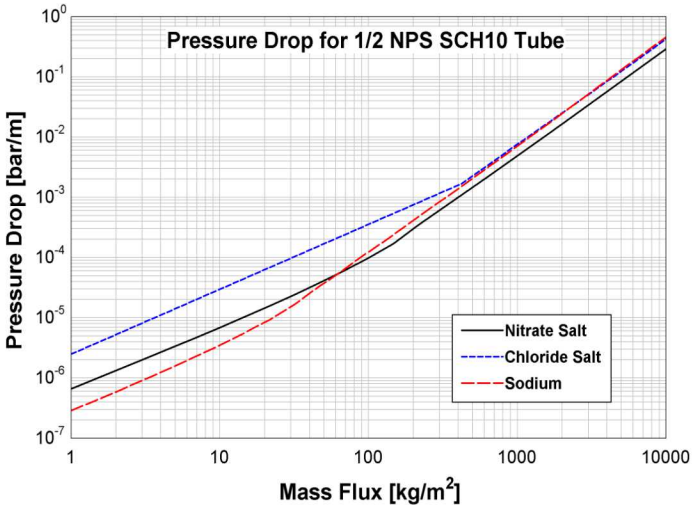

Figure 5. Pressure drop per meter of tube length for several fluids versus mass flux at 600 C and ambient pressure. The nitrate salt used is a mixture of 60% $NaNO_3$ and 40% KNO_3 and the chloride salt used is a mixture of 20% NaCl, 40% KCl, and 40% $MgCl_2$.

The receiver model in this work was created to capture broad trends in receiver efficiency. The receiver was subdivided into a series of equal length subsections along its height assuming a series of close-space vertical tubes in a once-through configuration and solved using the thermal resistance network model shown in Fig. 7. The internal EES "pipeflow" model was used to calculate forced internal flow correlations, where an external flow plate model was developed for calculating external convective loss coefficients assuming the tubes act similar to cross flow over a flat plate at a specified wind speed. These coefficients were used to calculate thermal resistance values and energy balances to determine resulting tube surface temperature and heat flow values. The results of this model compared with the receiver limit calculations are shown in Fig. 6, with relative error scaling with temperature from near 0 at low temperatures to between 50% and 100% at high temperatures. This behavior results from using the fluid inlet temperature to calculate the external convective heat transfer coefficient and radiative losses as these are dependent on the surface temperature being solved to avoid internal iteration in the model. However, when this model was used to calculate conditions of higher receiver efficiency, which occur at higher receiver surface temperatures, the resulting error was found to increase significantly.

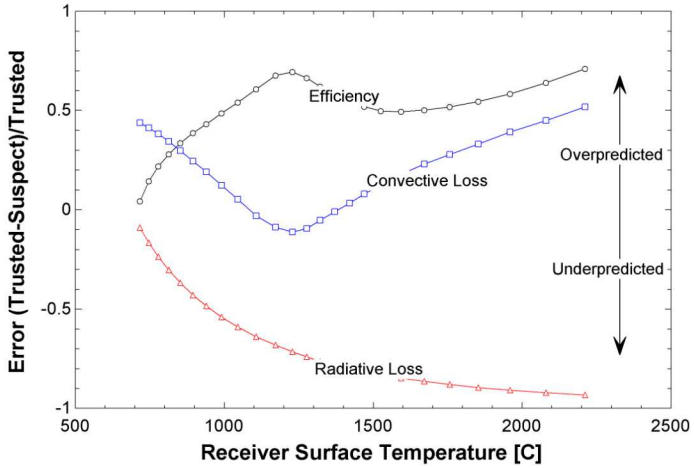

Figure 6. Comparison of solar to thermal efficiency, convective loss, and radiative loss error between the preliminary model (suspect) and the high-level model (trusted).

A revised discretized receiver model was created to address the excessive error in a previous preliminary model [6] so that sufficient accuracy and precision could be obtained to conduct preliminary receiver design.

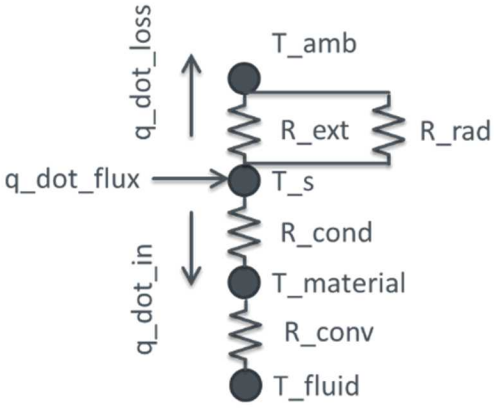

Figure 7. The simplified thermal resistance network for a subsection of the tubular receiver.

The basis of the model is a simplified thermal resistance network representing a bank of tubes with a given width and height as shown in **Error! Reference source not found.**. This subfunction is formulated to solve the reverse problem where all

temperatures are known so that temperature-dependent properties and correlations can be computed to solve for the heat into the receiver and lost from the receiver due to convection and radiation. The fluid, tube material, and surface temperatures are assumed to be the averages across the receiver (or section of the receiver) being modeled so for non-uniform incident flux or variable fluid properties a spatially discretized scheme should be used. In addition, the projected surface area of the receiver section is used to calculate each thermal resistance as shown in Eqns. 3-10.

$$R_{conv} = \frac{1}{h_{conv} A_s} \tag{3}$$

$$R_{cond} = \frac{th}{k_{mat} A_s} \tag{4}$$

$$R_{ext} = \frac{1}{h_{ext} A_s} \tag{5}$$

$$R_{rad} = \frac{T_s - T_{amb}}{q_{rad}" A_s} = \frac{T_s - T_{amb}}{A_s \varepsilon \sigma T_s^4} \tag{6}$$

$$R_{net,in} = R_{cond} + R_{conv} \tag{7}$$

$$R_{net,out} = \frac{1}{\frac{1}{R_{ext}} + \frac{1}{R_{rad}}} \tag{8}$$

$$\dot{q}_{in} = \frac{T_s - T_f}{R_{net,in}} \tag{9}$$

$$\dot{q}_{out} = \frac{T_s - T_{amb}}{R_{net,out}} \tag{10}$$

The external convection coefficient used for the receiver model assumed forced convection with a wind direction between incident and parallel flows to the plane of the receiver to characterize the worst-case scenario during operation. Correlation sub-routines: "External_flow_verticalplate" and "external_flow_plate" were used in EES for straight-on (0 deg) and cross-flow (90 deg), respectively, with a blending function shown as Eqn. 11 to account for wind angles between 0 and 90 degrees. The results of this blending function for various wind angles and wind speeds of 5 and 25 mph are shown in Fig. 8.

$$h_{ext} = \sqrt{\frac{\theta}{90\ [deg]} h_{cross}^2 + \frac{90\ [deg] - \theta}{90\ [deg]} h_{perp}^2} \tag{11}$$

The modeling architecture used in this analysis assumes that boundary conditions except for downstream thermal-hydraulic conditions are known as inputs to the model, so the solution of the thermal resistance network is fully implicit with the surface temperature being unbounded and highly sensitive to other parameters. The solution procedure therefore uses a combination of an exponential search to identify a reasonable maximum surface temperature bound followed by a binary search to identify the actual surface temperature using the thermal resistance network model and specified boundary conditions.

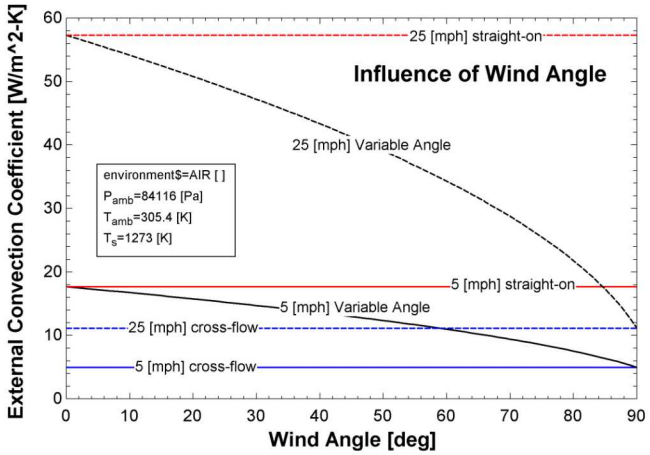

Figure 8. Effect of variable wind angle relative to the receiver plane demonstrating blending function.

Finally, a parametric study was performed using the tubular receiver model assuming the use of five nominal pipe sizes (1/8, ¼, 3/8, ½, ¾, and 1) with a Sch 10 wall thickness for various values of incident flux and different numbers of tube passes assuming the same values for ambient conditions, wind speed and direction (straight-on), and flow rates of 9.6 kg/s for the ternary salt and 8 kg/s for liquid sodium representing a temperature rise from 500 to 700 °C. A lumped capacitance approach was used so the average fluid temperature is set to 600 °C. A golden section search optimization routine was used to obtain a design for the receiver that absorbed 2 MWth in the specified number of tube passes.

The efficiency and receiver surface temperatures of the resulting designs obtained were plotted in Fig. 9 and show the same trend as was observed in Figure 1 for various levels of incident flux.

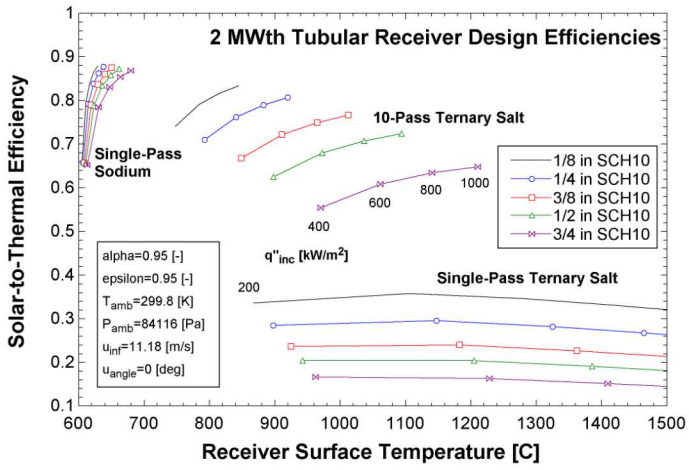

Figure 9. Efficiency versus surface temperature for a several ternary salt and sodium receiver designs.

However, because the mass flux, and therefore the internal convective heat transfer coefficient vary between each model, the trend between each level of incident flux for the same nominal pipe size didn't match the trend for constant internal convection coefficient. High receiver efficiencies up to 80% with modest surface temperatures up to 900 °C may be however possible for the ternary salt based on this model but would require very small tube diameters in a multi-pass arrangement which may prove impractical from a manufacturing or operational standpoint using traditional techniques. High efficiency sodium receivers, however, are much more practical as would be expected due to their higher heat transfer coefficients. In addition, there is far less spread in the designs of sodium receivers with the primary driver being the incident flux.

While high efficiencies may be possible, they can come at a cost of high pressure drops as shown in Fig. 10. However, moving toward larger tubes to reduce the pressure drop reduces receiver efficiency and leads to larger required receiver aperture areas. More passes would allow for larger and more practical tube sizes but still complicates fabrication due to the added bends and need for thermally compliant tube supports. It also increases the risk that any entrained ullage gas, salt vapor, or air could vapor-lock one of the receiver passes and lead to tube burnout and rupture, so peak vents would need to be provided to ensure proper filling and purging of any trapped gasses.

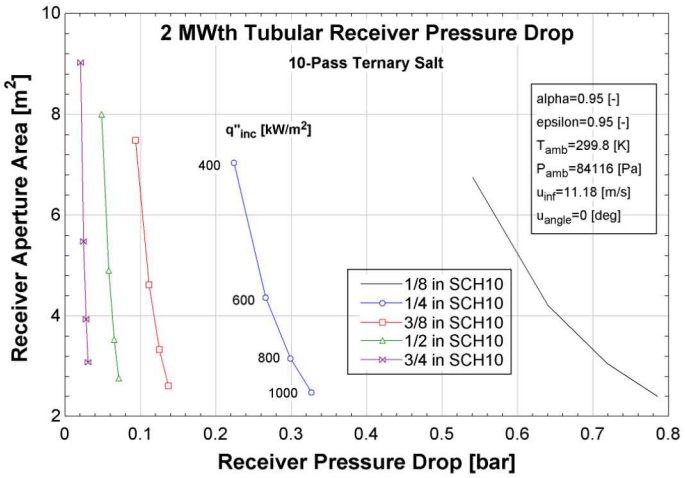

Figure 10. Receiver pressure drop and aperture area versus pipe size and heat flux for ternary salt.

3.2. Thermal-Transport Characterization

Similar to work performed by Armijo et al. [6], system analysis for this investigation explored predicted dynamic head losses as a function of respective cold and hot pump flow rates. Ideal system pump curves were calculated and recirculation for each respective tank was assessed by a designed throttle valve with a determined C_v value. Pump designs for the cold and hot-leg pumps estimated the operating range for the two pumps to be between 1800 and 2400 RPM. The process flow design, Fig. 2 has approximately 400 ft. and 433 ft. of 2.5 in. ID Sch. 80 piping for the hot and cold lines respectively. Calculations of flow head, along with initial pump designs estimated both hot and cold pump nominal flow rates to be as high as 110 GPM to meet requirements for steady operation. A 2400 RPM pump curve was used to provide operational metrics. The speed calculated for a long-shafted pump, based on an approximated dead-head of 119 ft and 352 ft, and a best efficiency point (BEP) head of 90 ft and 302 ft for the cold and hot pumps respectively. Recirculation control studies were performed where it was found that the cold recirculation mass fraction range was between 0.026 to 0.28 and the hot recirculation mass fraction was between 0.27 to 0.61.

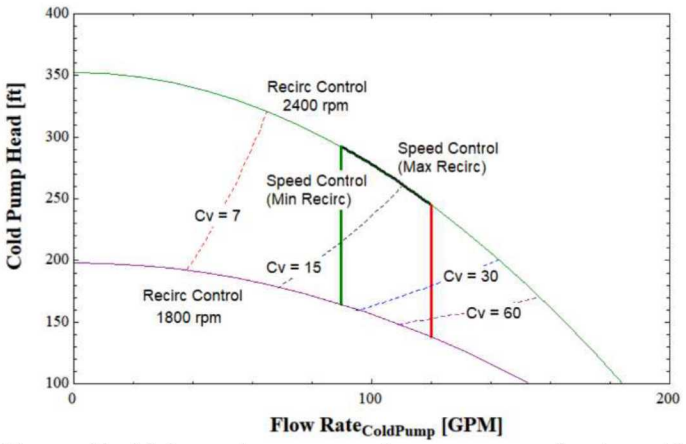

Figure 11. Molten salt system and pump curves for the cold pump.

As shown in Fig. 11 the operating envelope had a maximum speed control of the recirculating throttle valve as well as 1800 and 2400 RPM pump operating limits. For 2400 RPM, respective hot pump TDH values were determined to be 260.1-307 ft. for pump flow rates of 90-120 GPM. The results also suggest a recirculating throttle valve minimum C_v of 60 required to meet the operational envelope spanning the RPM range considered here.

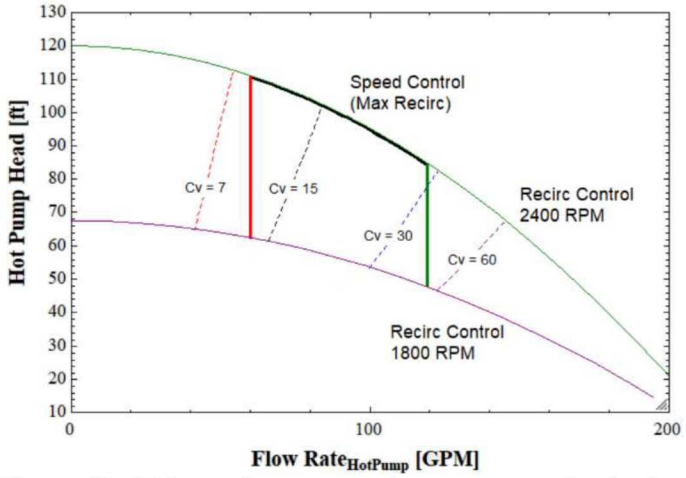

Figure 12. Molten salt system and pump curves for the hot pump.

For the hot pump, Fig. 12 results suggest TDH values between 88.18-115.1 ft. for 2400 RPM. For this pump a minimum *C*v of 30 was determined for the hot-side throttle recirculation valve for the operational envelope assessed here. For both throttle recirculation valves, high *C*v values will be required for this configuration with minimal pressure drops. This necessitates pump operating points with minimal recirculation.

4. CONCLUSION

A rigorous thermodynamic system model was developed using EES to assess operational modes for a 2.0-MWth liquid-heat transfer system test loop with a ternary chloride molten-salt TES. This work investigated receiver performance and efficiency comparisons between the ternary chloride salt and sodium as the HTF. From the model, the HTC and pressure drop per unit length of a liquid were found to vary primarily with mass flux and to a lesser extent with temperature, pressure, and flow geometry. Here, depending on the height and configuration of the receiver, the pressure drop per unit length allowed will range from 0.1 bar/m to 0.5 bar/m resulting in expected mass fluxes between 3000 kg/m^2 and 10000 kg/m^2 because the pressure drop of the three fluids considered is fairly similar. Comparison of the sodium with the ternary chloride salt, as well as with nitrate solar salt found results suggesting HTCs with nitrate salts ranging from 8,000 to 20,000 W/m^2-K, chloride salts ranging from 3,000 to 9,000 W/m^2-K, and sodium ranging from 30,000 to 60,000 W/m^2-K. Further receiver modelling results found that moving toward larger tubes to reduce the pressure drop reduces receiver efficiency and leads to larger required receiver aperture areas. More passes would allow for larger and more practical tube sizes but still complicates fabrication due to the added bends and need for thermally compliant tube supports. Finally, from the system TES analysis, recirculation control studies performed found that the cold recirculation mass fraction range was between 0.026 to 0.28 and the hot recirculation mass fraction was between 0.27 to 0.61. For a pump speed of 2400 RPM, respective hot pump TDH values were determined to be 260.1-307 ft. for pump flow rates of 90-120 GPM. For the cold pump at the same mass flow rate and pump speed, the TDH was determined to be 260.1-307 ft. The *C*v's determined for the cold and hot recirculation valves were determined to be 30 and 60 respectively.

ACKNOWLEDGEMENTS

Sandia National Laboratories is a multi-mission laboratory managed and operated by National Technology & Engineering Solutions of Sandia, LLC, a wholly owned subsidiary of Honeywell International Inc., for the U.S. Department of Energy's National Nuclear Security Administration under contract DE-NA0003525.

REFERENCES

[1] Asselineau, C.A., Venn, F., Logie, W., Potter, D., Kim, J.S., Pye J. and Coventry, J., "Design of ASTRI's high-temperature liquid sodium receiver prototype," Proceedings of SolarPACES2019, 2019.

[2] Ho, C. K., & Iverson, B. D., "Review of high-temperature central receiver designs for concentrating solar power", Renewable and Sustainable Energy Reviews, 29, pp. 835-846, 2014.

[3] Coventry, J., Andraka, C., Pye, J., Blanco, M. and Fisher, J., "A review of sodium receiver technologies for central receiver solar power plants," Solar Energy, 122, pp.749-762, 2015.

[4] M. Mehos, C. Turchi, J. Vidal, M. Wagner, Z. Ma, C.K. Ho, W. Kolb, C. Andraka, and A. Kruizenga, "Concentrating Solar Power Gen3 Demonstration Roadmap," NREL/TP-5500-67464, NREL, 2017.

[5] Pacio, J., Wetzel, T., "Assessment of liquid metal technology status and research paths for their use as efficient heat transfer fluids in solar central receiver systems," Sol. Energy 93, 11–22, 2013.

[6] Armijo, K.M., Carlson, M.D., Dorsey, D.S., Ortega, J.D., Madden, D., Coventry, J. and Turchi, C., "Operational Modes of a 2.0 MWth Chloride Molten-Salt Pilot-Scale System," 23rd SolarPACES Conference, Daegu, South Korea, 2019.

[7] Ho, C.K., "Advances in central receivers for concentrating solar applications," Sol. Energy, vol. 152, pp. 38–56, 2017.